Dysregulated miR-125a promotes angiogenesis through enhanced glycolysis

Check for updates

Sarah M. Wade [a,b], Nils Ohnesorge [b], Hayley McLoughlin [a], Monika Biniecka [b], Steven P. Carter [c], Michelle Trenkman [b], Clare C. Cunningham [a,b], Trudy McGarry [a,b], Mary Canavan [a,b], Breandán N. Kennedy [c], Douglas J. Veale [b], Ursula Fearon [a,b,*]

[a] Molecular Rheumatology, School of Medicine, Trinity Biomedical Sciences Institute, Trinity College Dublin, Dublin 2, Ireland
[b] EULAR Centre for Arthritis and Rheumatic Diseases, Vincent's University Hospital, Dublin Academic Health Care, University College Dublin, Dublin 4, Ireland
[c] UCD School of Biomolecular & Biomedical Science, UCD Conway Institute, University College Dublin, Belfield, Dublin 4, Ireland

ABSTRACT

Background: Although neoangiogenesis is a hallmark of chronic inflammatory diseases such as inflammatory arthritis and many cancers, therapeutic agents targeting the vasculature remain elusive. Here we identified miR-125a as an important regulator of angiogenesis.
Methods: MiRNA levels were quantified in Psoriatic Arthritis (PsA) synovial-tissue by RT-PCR and compared to macroscopic synovial vascularity. HMVEC were transfected with anti-miR-125a and angiogenic mechanisms quantified using tube formation assays, transwell invasion chambers, wound repair, RT-PCR and western blot. Real-time analysis of EC metabolism was assessed using the XF-24 Extracellular-Flux Analyzer. Synovial expression of metabolic markers was assessed by immunohistochemistry and immunofluorescent staining. MiR-125a CRISPR/Cas9-based knock-out zebrafish were generated and vascular development assessed. Finally, glycolytic blockade using 3PO, which inhibits Phosphofructokinase-fructose-2,6-bisphophatase 3 (PFKFB3), was assessed in miR-125a−/− ECs and zebrafish embryos.
Findings: MiR-125a is significantly decreased in PsA synovium and inversely associated with macroscopic vascularity. In-vivo, CRISPR/cas9 miR-125a$^{-/-}$ zebrafish displayed a hyper-branching phenotype. In-vitro, miR-125a inhibition promoted EC tube formation, branching, migration and invasion, effects paralleled by a shift in their metabolic profile towards glycolysis. This metabolic shift was also observed in the PsA synovial vasculature where increased expression of glucose transporter 1 (GLUT1), PFKFB3 and Pyruvate kinase muscle isozyme M2 (PKM2) were demonstrated. Finally, blockade of PFKFB3 significantly inhibited anti-miR-125a-induced angiogenic mechanisms in-vitro, paralleled by normalisation of vascular development of CRISPR/cas9 miR-125a$^{-/-}$ zebrafish embryos.
Intepretation: Our results provide evidence that miR-125a deficiency enhances angiogenic processes through metabolic reprogramming of endothelial cells.
Fund: Irish Research Council, Arthritis Ireland, EU Seventh Framework Programme (612218/3D-NET).

1. Introduction

PsA is a multi-faceted chronic inflammatory disease which effects musculoskeletal structures, skin and nails [1]. This heterogeneous presentation has led to difficulties with effective treatment, with 40% of patients failing to respond optimally [2], emphasizing the need for new strategies. A key pathogenic event in PsA pathophysiology, irrespective of disease location, is aberrant blood vessel growth, which orchestrates the persistent infiltration of immune cells and the transition into chronic inflammation [3,4]. Previous studies have shown a distinct macroscopic vascular pattern, characterized by elongated, tortuous and dilated vessels compared to patients with rheumatoid arthritis (RA) [5,6]. This vascular pattern is associated with differential synovial expression of the angiogenic growth factors; vascular endothelial growth factor (VEGF), its receptors VEGFR-1/Flt1 and VEGFR-2/KDR, Angiopoietin (Ang) 1 and 2 and their receptor Tie2 at both early and late disease stages [7,8], which correlate with disease activity and radiographic progression [9,10].

Though anti-VEGF treatment has proven successful in the treatment of age-related macular degeneration [11], blockade of angiogenic growth factors has largely failed in other complex diseases, such as

* Corresponding author.
E-mail address: fearonu@tcd.ie (U. Fearon).

Research in context

Evidence before this study

We considered all the relevant evidence on angiogenesis and the role that MiRNA plays in its regulation, and in the pathogenesis of many inflammatory diseases and cancers. Previous studies have implicated miR-125a in disease pathogenesis due to its ability to regulate numerous targets, however not specifically angiogenesis and metabolism. Our search strategy used the following terms 'angiogenesis' 'microRNA' and 'metabolism' in PubMed to include those reports published in the English language between June 30, 1988 and Jan 31, 2019. We prioritised original articles that related to the search terms in studies of human health.

Added value of this study

We elucidate a specific role for miR-125a in the regulation of angiogenesis relevant to inflammatory diseases, namely Psoriatic Arthritis (PsA), in which expression appears to be reduced in the joint lining synovial tissue. In addition, we show that levels correlate with increased vascularity in the joint. In parallel miR-125a deficiency resulted in endothelial cell activation and a distinct metabolic shift towards glycolysis. Using CRISPR/Cas9 techniques, we demonstrate loss of miR-125a in zebrafish embryos results in a hypervascular phenotype. Finally, we demonstrate that the effect of miR-125a deficiency on endothelial cell activation is reversed when glycolysis is inhibited, following PFKFB3 blockade both *in vitro* and *in vivo*.

Implications of all the available evidence

This is the first report of a role for MiR-125a in the regulation of angiogenesis, *via* an effect on endothelial cell metabolism, with specific relevance to a common inflammatory disease impacting on human health. These data suggest that the miR-125a-glycoylsis axis represents a novel opportunity for intervention of inflammatory arthritis and other angiogenesis-related diseases.

cancer, due to resistance and toxicity [12]. Therefore, there is an urgent need for novel anti-angiogenic strategies. It has recently been shown that endothelial cell metabolism and metabolic reprogramming are key features of vessel sprouting and tumour angiogenesis [13,14]. Activated endothelial cells increase their rates of glycolysis to enable the rapid generation of ATP necessary to meet the energy demands for cell migration, cell extension and proliferation for new vessel formation [15]. Under conditions of inflammation and tumorigenesis, targeted inhibition of specific glycolytic enzymes in stromal, endothelial and immune cells resolves chronic inflammation and prevents tumour metastasis and tumour survival [16–18]. However, despite the increasing attention to the role of glycolysis in angiogenesis driven tumours, the impact and/or regulation of glycolysis-induced angiogenesis in arthritis is not well understood.

Numerous studies have demonstrated the role of miRNA in a range of processes including angiogenesis, metabolism and immune cell activation; hence have been implicated in the pathogenesis of a number of autoimmune diseases [19–22]. As dysfunctional angiogenesis is a key pathogenic event in the development and progression of PsA, we investigated the effect of aberrant miRNA expression on endothelial cell function, cellular metabolism, gene expression and its contribution to pathological angiogenesis. Our data show a down-regulation of miR-125a in PsA synovial tissue, which is associated with joint angiogenesis. In addition, we show an increase in metabolic markers in PsA synovial vasculature compared to non-inflamed tissue. miR-125a deficiencies resulted in endothelial activation through metabolic reprogramming and

elevated glycolysis, inducing endothelial cell sprouting *in vitro* and *in vivo*. Furthermore, our data suggest that the targeted inhibition of glycolysis can normalise miR-125a$^{-/-}$-induced dysfunctional sprouting and may provide a novel approach in treating angiogenesis-driven chronic inflammatory conditions such as PsA.

2. Methods

2.1. Patient recruitment

Patients with active inflammatory arthritis were recruited from outpatient clinics at the Department of Rheumatology, St. Vincent's University Hospital (Dublin, Ireland). All patients met the CASPAR diagnostic criteria [51]. Arthroscopy of the inflamed knee was performed under local anaesthetic using a 2.7 mm needle arthroscope (Richard Wolf, Illinois, USA). Macroscopic vascularity was assessed under direct visualisation and scored as described previously [5]. Demographic and clinical information are detailed in Table S1. For immunohistochemical and miRNA analysis, synovial tissue biopsy samples were immediately embedded in mounting media or snap frozen in liquid nitrogen. Peripheral blood mononuclear cells were also obtained at arthroscopy and were isolated according to standard procedures. All patients provided written informed consent as approved by the local Ethics Committee of St. Vincent's University Hospital.

2.2. Quantitative real-time PCR

Total RNA was extracted using miRNeasy Kit (Qiagen). Mature miRNA expression was quantified using specific primers designed for hsa-miR-125a, hsa-miR-125b, dre-miR-125a, dre-miR-125b-5p, dre-miR-125b-1-3p, dre-miR-125b-2-3p and miR-125b-3p with a universal reverse sequence primer as described previously [52]. For mRNA analysis, cDNA was synthesized with high-capacity cDNA reverse transcription kit (Applied Biosystems). qPCR was performed with SYBR green qPCR master mix (Applied Biosystems) with specific primers (Table S1). Relative gene expression was normalised to the expression of the house keeping gene; ribosomal protein lateral stalk subunit P0 (RPLP0). Principle Component Analysis (PCA) was performed on scaled log$_2$ expression values using the prcomp function in R (Version 3.3.1).

2.3. Cell culture and treatment

Human Umbilical Vein Endothelial Cells (HUVEC) (Lonza) were incubated in MCDB (Gibco) media supplemented with L-glutamine (Gibco-BRL), 0.5 ml EGF (Gibco-BRL), 50 ml FCS (Gibco-BRL), 0.5 ml hydrocortisone, penicillin (100 units/ml; Bioscience), streptomycin (100 units/ml; Bioscience) and fungizone (0.25 µg/ml; Bioscience). Cells were cultured at 37 °C in humidified air with 5% CO2 and harvested with trypsin-EDTA (Lonza). HUVEC were transfected at 70–80% confluence with 100 nM anti-miR-125a or anti-control (Ambion) using lipofectamin 2000 (Invitrogen) as per manufacturer's instruction. Twenty-four hours after transfection, the medium was changed to fresh complete MCDB and treated where indicated with 3PO (20 µM) or DMSO (20 µM) for 24 h.

2.4. Migration and transwell invasion assay

For wound healing assays, HUVECs were cultured in 48-well plates at 70–80% confluence. Following 24 h transfection under the specified conditions, a wound was scratched in the centre of the cell monolayer by a sterile plastic pipette tip and debris was removed by PBS washing. Transwell invasion assays were performed in Corning Matrigel Invasion Chamber inserts (8.0 µM pore size, Corning) at 3×10^4 cells/insert in the upper chamber. Cells were allowed to migrate/invade for 24 h at 37 °C. For the transwell invasion assay, non-invading cells were removed from the upper surface of the chamber. Cells were fixed with 1%

paraformaldehyde and stained with 0.1% crystal violet and the number of migrating/invading cells were quantified as previously described [53].

2.5. Tube formation assay

HUVECs were seeded on growth factor-reduced Matrigel (BD Bioscience)-coated 96-well plates at 3×10^4 cells per well for 18–24 h. The endothelial tubule formation was observed and photographed using an inverted microscope. Number of tubes formed were manually counted. The number of branches, junctions and nodes were quantified using the Image J software.

2.6. Histological analysis

Immunohistochemistry analysis was performed using paraffin synovial tissue sections and the Dako ChemMate Envision Kit (Dako). Sections were made of 7 μm thickness, deparaffinised in xylene and rehydrated in alcohol and deionised water. Antigen retrieval was performed by heating sections in antigen retrieval solution (15 ml of 1 M sodium citrate and 15 ml of 1 M citric acid in deionised water, pH 6.0) in a pressure cooker. Slides were blocked with 10% casein in PBS for 20 min, and then incubated with primary antibodies; ATP5P (Santa Cruz Biotechnology), PFKFB3, (Abcam), PKM2 (Abgent), GLUT1 (Abcam), followed by a horseradish peroxidase-conjugated secondary antibody (Dako). An IgG1 control antibody (Dako) was used as a negative control. Colour was developed in diaminobenzidine solution (1:50; Dako) and counterstained with hematoxylin. Slides were mounted using Pertex media. Images were captured using Olympus DP50 light microscope and AnalySIS software (Soft Imaging System Corporation, Lakewood). Vascular regions were scored using a well-established semi-quantitative scoring method (0–4) as previously described [54,55]. Dual-immunofluorescent staining for PFKFB3 (Abcam) and vWF (DAKO) was performed on cryostat synovial sections. Synovial sections were fixed with acetone for 10 min and co-incubated with primary mouse antibody against human vWF and primary rabbit antibody against PFKFB3. Following incubation for 18 h, sections were stained with donkey anti-mouse AlexaFluor 647 (Abcam) and donkey anti-rabbit AlexaFlour 488 (Abcam) for 60 min and counterstained with 4′,6-diamidino-2-phenylindole (DAPI) nuclear stain (Sigma-Aldrich) for 2 min. Samples were mounted with Molecular Probes antifade mounting medium (Thermo Fisher Scientific) and assessed by immunofluorescence microscopy (Olympus BX51; Olympus, Hamburg, Germany).

2.7. Seahorse assay

An XF-24 Extracellular Flux Analyzer (Seahorse Bioscience) was used to analyse real-time changes of the two main energy pathways; oxidative phosphorylation and glycolysis. Transfected HUVEC were seeded in XF-24 well culture plates at 3×10^4 cells and allowed to adhere. Cells were rinsed and maintained in seahorse assay base medium with 10 mM glucose (pH 7.4) 1 h prior to assay initiation. Cells were treated with 2 μg/ml oligomycin, 5 μM FCCP and 2 μM antimycin A (Seahorse Bioscience). MRC rate as calculated by the decrease in OCR from baseline following oligomycin treatment. SPC rate as calculated as the increase in OCR compared to baseline following FCCP treatment.

2.8. Western blotting

Cells were scraped and centrifuged prior to cell lysis. Ice-cold RIPA (Radio-Immunoprecipitation Assay) buffer (Sigma, Missouri, USA) containing 10 μg/ml phosphatase inhibitor cocktail and 10 μg/ml protease inhibitor cocktail (Sigma) was used to extract protein from transfected HUVEC. Measurement of protein concentration was performed using a BCA assay (Pierce Chemical Co, Rockford, IL, USA). Protein (5 μg) was resolved on SDS-PAGE (5% stacking, 10% resolving), gels were then transferred onto PVDF membranes (Amersham Biosciences, UK) prior to 1 h blocking in wash buffer containing 3% BSA (0.1% Tween) with gentle agitation at room temperature. Membranes were incubated with mouse monoclonal anti-HK2 (Novus Biologicals, Colorado, USA) and rabbit monoclonal anti-PFKFB3 (Abcam, UK), and diluted in 3% BSA containing 0.1% Tween 20 at 4 °C overnight with gentle agitation. β-actin (1:5000, Sigma) was used as a loading control. Following three 15 min washes, membranes were incubated with appropriate horseradish peroxidase conjugated secondary antibodies (1:5000) for 3 h at RT. The signal was detected using SuperSignal® West Pico Chemiluminescent Substrate (Amersham Biosciences). Band densities were imaged using the ChemiDoc MP Imaging System (Bio-Rad, California, USA).

2.9. Zebrafish husbandry and hyperbranching analysis

Zebrafish maintenance and husbandry were as per standard conditions of 28 °C with a constant 14 h light/10 h dark lighting cycle. Embryos were kept in E3 medium (5 mM NaCl, 0.17 mM KCL, 0.33 mM $CaCl_2$, 5–10% methylene blue) at 28.5 °C with or without 0.003% 1-phenyl-2-thiourea (PTU) to inhibit pigment formation. Embryos of the Tg(fli1:EGFP)^{y1} line were used for vasculature analysis. For 3PO experiments, embryos were placed into 6-well plates with E3 medium, to which 3PO (30 μM) or DMSO vehicle control (30 μM) was added 3 days post fertilization (dpf) for 48 h. All protocols were approved by the local government authority, Health Products Regulatory Authority (license no: AE18982/P062). Embryos were scored according to severe (1–2 ISVs with interesting hyperbranches), moderate (1–2 mid-length intersecting hyperbranches), mild (1–2 small hyperbranches) and no (no hyperbranches).

2.10. Morpholinos

Antisense morpholino oligonucleotides (MOs) were obtained from Gene Tools (Fig. S2 for morpholino coverage over each member of the miR-125 family). The following pre-miRNA processing, blocking and control morpholino were used; miR-125-MO targeted sequence: 5' AAACGTCACAAGTTAGGGTCTCAGG 3', Control MO scrambled sequence: 5' CCTCTTACCTCAGTTACAATTTATA 3'. Antisense MO oligonucleotides were diluted in water to give a stock concentration of 8.3 μg/μl. Microinjections of 5–6 ng of the MO were performed at the 1–2 cell stage using a Nanoliter 2000 injector together with a Sys-Micro4 controller (World Precision Instruments).

2.11. Generation of the miR-125a1$^{-/-}$ mutant line

CRISPR target sites were identified using ZiFiT Targeter program (Version 4.1) [56,57] as previously described [58]. The target sequences for miR-125a1 are as follows; GGGTGCAGAGGGGTGATCCA and CCTGAG GTCCTCAGGAACA. Targeted guide strand RNA were generated using a pDR275 guide RNA expression vector (Addgene, Keith Joung Lab). WT (Tubingen strain) embryos were injected (1 nl) at the 1 cell stage with a 1:2 mix of Cas9 mRNA and miR-125a1 targeted guide RNA duplex and raised to adulthood. F0 founder fish were identified and outcrossed with Tg(fli1:EGFP)^{y1} to generated miR-125$^{+/-}$ Tg(fli1:EGFP)^{y1} F1 progeny. DNA from tail fins was extracted, amplified and sequenced to identify heterozygous F1 Tg(fli1:EGFP)^{y1}. miR-125a1$^{+/-}$ were selfcrossed to generate F2 embryos which were used until 4 dpf in the outlined experiments following genotype identification (Table S2 Primer Sequences).

2.12. Statistical analysis

Wilcoxon Signed Rank test or Mann Whitney was used for analysis of non-parametric data. Student t-test was used for parametric data, Fishers exact test for phenotype frequency and Chi-square test for

phenotype severity. Spearman's rank correlation was performed to correlate the synovial tissue expression of miR-125a and macroscopic joint vascularity. Area under the receiver operating characteristic (ROC) curve (AUC) with 95% confidence interval (CI), sensitivity was calculated to determine the accuracy index for evaluating the ability of miR-125a synovial tissue expression to distinguish macroscopic joint vascularity. All analysis were performed using GraphPad Prism (Version 5). *P*-values of <0.05 (*p < .05) were determined as statistically significant.

3. Results

3.1. miR-125a is downregulated in PsA synovial tissue and is associated with joint angiogenesis

Previous miRNA studies in PsA have largely focused on peripheral blood expression profiles [23,24]. However, emerging evidence strongly supports tissue-specific miRNA profiles which mediate disease site-specific pathogenic mechanisms. We therefore investigated the expression of the miR-125a family members, miR-125a and miR-125b, both being previously associated with dysfunctional angiogenesis [25,26], in peripheral blood cells and inflamed synovial tissue obtained from PsA patients with active disease and compared them to osteoarthritis

(OA), disease comparator. miR-125a and miR-125b were significantly increased in PsA peripheral blood compared to OA peripheral blood cells (Fig. 1A). In contrast, PsA synovial tissue showed a significant decrease in miR-125a and miR-125b expression compared to OA disease comparator (Fig. 1B).

To identify the potential pathogenic function of aberrant miR-125 expression in the PsA synovial tissue, miR-125a and miR-125b expression levels were assessed in relation to synovial markers of disease (disease activity scores, synovitis and vascularity), demonstrating a trend towards a negative correlation between synovial tissue expression of miR-125a and joint vascularity ($r = -0.5$; $p = .104$) (Fig. 1C). The classification of samples into low miR-125 (<1.5 -delta ct) and high miR-125a (>1.5 -delta ct), demonstrates a significant increase in synovial macroscopic vascularity (1–100) in patients with low synovial expression of miR-125a as compared to patients with high synovial expression of miR-125a (Fig. 1D and E). Receiver operating characteristics (ROC) analysis demonstrated the specificity and sensitivity of miR-125a in separating PsA patients according to joint vascularity (Fig. 1F; Area Under the Curve: 0.68). miR-125b expression did not show any association with disease activity and was not examined further (data not shown). Collectively, these data suggest a potential role for miR-125a in the regulation of joint angiogenesis in PsA.
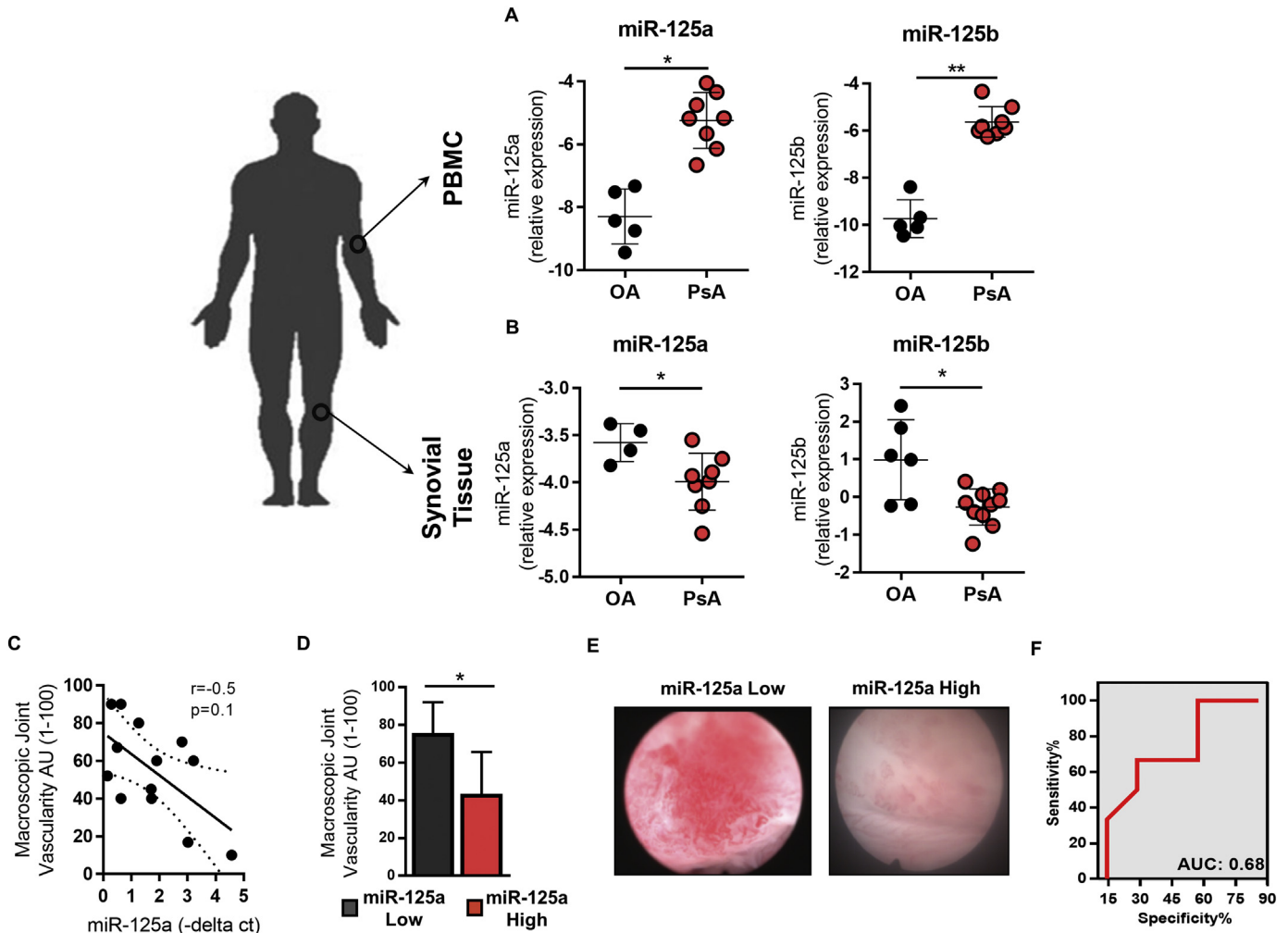

Fig. 1. miR-125a expression is decreased in PsA synovial tissue and associated with joint angiogenesis. The relative expression of miR-125a and miR-125b in PsA (A) peripheral blood mononuclear cell (PBMC) ($n = 7$) and (B) synovial tissue ($n = 8$) *versus* OA controls ($n = 4$–6). Data are represented as –delta ct median with interquartile range compared to endogenous control RNU48. (C) Synovial expression of miR-125a were plotted against macroscopic vascularity. (D) Bar chart quantifying synovial angiogenesis (score 1–100) in patients grouped according to low *versus* high joint expression of miR-125a. Data are represented as standard error of the mean. (E) Representative arthroscopy images of macroscopic vascularity of a patient with low *versus* high joint expression of miR-125a. (F) Area Under the Curve (AUC) was calculated with 95% confidence limits based on miR-125a synovial expression and macroscopic joint vascularity. *$p < .05$ significantly different across groups.

3.2. miR-125a regulates endothelial cell migration, invasion and tube formation

To elucidate the role of miR-125a on endothelial cell (EC) function, EC were transfected with miR-125a antisense oligonucleotides and EC activation assays were performed. Reduction of mature miR-125a levels in silenced cells was confirmed by RT-PCR (Figs. S1A and S1B). To study the effect of miR-125a on vessel branching, we performed two dimensional tube formation assays. miR-125a knockdown significantly induced vessel network formation (Fig. 2A and B), paralleled by increased frequencies of branching points, junctions and nodes (Fig. 2B). Anti-miR-125a treated ECs also significantly increased migration (Fig. 2C and D) and promoted invasion (Fig. 2E and F). Supporting this finding, increased expression of miR-125a significantly inhibited EC branching and motility (Figs. S1C, S2A and S2b). To better understand the molecular mechanisms of miR-125a deficiency on ECs, we performed transcriptional analysis of anti-miR-125a treated ECs as compared to control transfected cells. Gene expression analysis revealed anti-miR-125a treated ECs upregulate a number of genes related to EC activation (Fig. 2G). Consistent with the functional phenotype, genes associated with vessel branching, migration and invasion were over-expressed in anti-miR-125a treated ECs, including VEGFA, YAP, ANG2, MMP2 and RAC (Fig. 2H). This demonstrates that EC morphology and function are regulated, at least in part, by miR-125a.

3.3. Silencing of miR-125 in Zebrafish causes vascular hyperbranching

We next explored the functional role of miR-125a in vascular development using both morpholino and CRISPR/Cas9 technology. It is noteworthy that the mature miR-125a sequence is strongly conserved across different species, including zebrafish, and share an identical seed sequence supporting the functional importance for miR-125a (Fig. S3A). One widely used tool for the transient knockdown of specific miRNA in zebrafish is morpholino (MO) antisense technology, which prevent miRNA maturation by binding to the Drosha site, Dicer site and the mature microRNA strand resulting in the blockade of
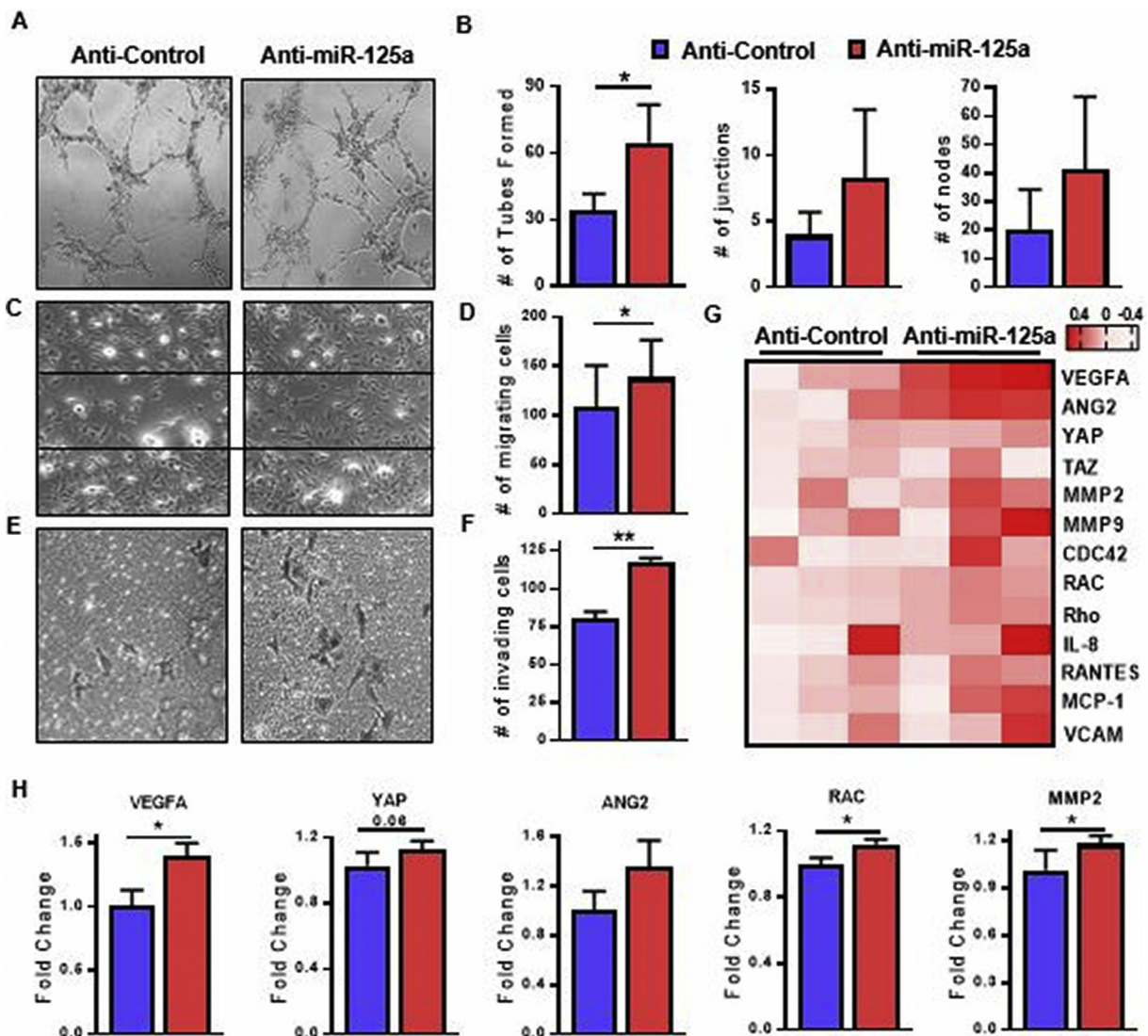

Fig. 2. miR-125a promotes endothelial cell activation. Representative images of (A) demonstrating HUVEC network formation in response to anti-miR-125 and scrambled controls ($n = 3$). (B) Bar graphs quantifying the number of tubes formed, branching points, junctions and nodes per high power field. (C) Representative photomicrographs demonstrating HUVEC wound repair assay in response to anti-miR-125a treatment compared to anti-control ECs ($n = 3$). (D) Bar graphs quantifying the number of migrating cells as counted in five random fields of vision. (E) Representative photomicrographs demonstrating HUVEC invasion in response to anti-miR-125 and scrambled controls ($n = 3$, original magnification 10×). (F) Bar graphs quantifying the number of invading cells as counted in five random fields of vision. (G) Heatmap displaying the gene transcripts for the main molecular markers of endothelial cell activation as quantified by RT-PCR ($n = 6$), heatmap is presented as $\log_2$ values. (H) Gene sets of endothelial cell branching, migration and invasion compared in 3 anti-control/anti-miR-125a pairs. Relative gene expression measured by RT-PCR (n = 3). Data are represented as mean ± SEM. ** $p < .01$, * $p < .05$ significantly different compared to control. See also Fig. S1 and S2.

pre-microRNA processing. The miR-125 family has six orthologues in zebrafish; miR-125a1, miR-125a2, miR-125b-5p, miR-125b-1-3p, miR-125b-2-3p and miR-125b-3-3p, with similar Drosha, Dicer and seed sequences (Fig. S3B), therefore making it difficult to selectively and specifically inhibit individual family members. We therefore designed and injected a single miR-125-MO targeting all members of the miR-125 family into Tg(fli1:EGFP)^{y1} transgenic zebrafish and analysed vascular development. At 1, 2 and 4 days post-fertilization (dpf), 50% of morphants injected with miR-125-MO showed gross morphological aberrations and clear developmental impairment (Fig. S3C), resulting in 53% embryo death in miR-125 morphants, versus 6% of control embryos. Compared to control-MO injected embryos, miR-125-MO embryos showed a significant reduction (60–70%) in miR-125 expression, supporting the efficacy of MO-mediated blockade of miR-125 (Fig. S4A). Formation of the major vessels in the zebrafish trunk were examined at 4 dpf in the surviving larvae and were found to be normal in the control-MO injected larvae. In contrast, 50% of the miR-125 morphants displayed excessive branching of the intersegmental vessels (ISV) (Fig. S4B). Other vessels in the zebrafish trunk; dorsal aorta, dorsal longitudinal anastomotic vein and posterior cardinal vein developed normally.

To dissect the specific contribution of miR-125a in vascular development and to overcome the unspecific effects associated with morpholino injection, we used the CRISPR/Cas9 technology to generate miR-125a1$^{-/-}$ zebrafish. As depicted in Fig. 3A, Cas9 target sites were identified 5′ and 3′ of the miR-125a1 gene in a genomic location devoid

of protein coding genes. CRISPR guide RNAs (gRNA) with tracrRNA were generated to selectively guide the Cas9 protein to these genomic locations. Tg(fli1:EGFP)^{y1} miR-125a$^{+/-}$ heterozygous zebrafish were incrossed to generate miR-125a1$^{-/-}$ embryos as identified by Sanger sequencing and genotyping (Figs. 3B and S5A). In contrast to morpholino-mediated blockade of miR-125a, there was no evidence of elevated mortality in miR-125a1$^{+/+}$, miR-125a1$^{+/-}$ or miR-125a1$^{-/-}$ embryos, with normal Mendelian inheritance being observed (Fig. 3C). Furthermore, miR-125a1$^{+/-}$ and miR-125a1$^{-/-}$ embryos showed no defects in gross morphology or development rates compared to miR-125a1$^{+/+}$ embryos (Fig. S5B). In contrast to this, hyper-branching phenotypes were observed at 4 dpf in all miR-125a1$^{-/-}$ larvae, where 33% displayed a mild phenotype, 45% displayed a moderate phenotype and 22% exhibited a severe ISV hyper-branching phenotype (Fig. 3D). Collectively, these data suggest that miR-125a is an important regulator of vascular sprouting.

3.4. Loss of miR-125a induces metabolic reprogramming in endothelial cells

In recent years, we and others have demonstrated the fundamental role of EC glycolysis in angiogenesis [14,27–29]. To assess the potential role of dysregulated metabolism in PsA synovial vasculature, we first examined the expression of surrogate markers of metabolism; GLUT1, PFKFB3, PKM2 and ATP5P in PsA synovial tissue sections. Analysis of the synovial vascular regions demonstrated significantly greater expression of GLUT1, PFKFB3, PKM2 and ATP5B in PsA synovial
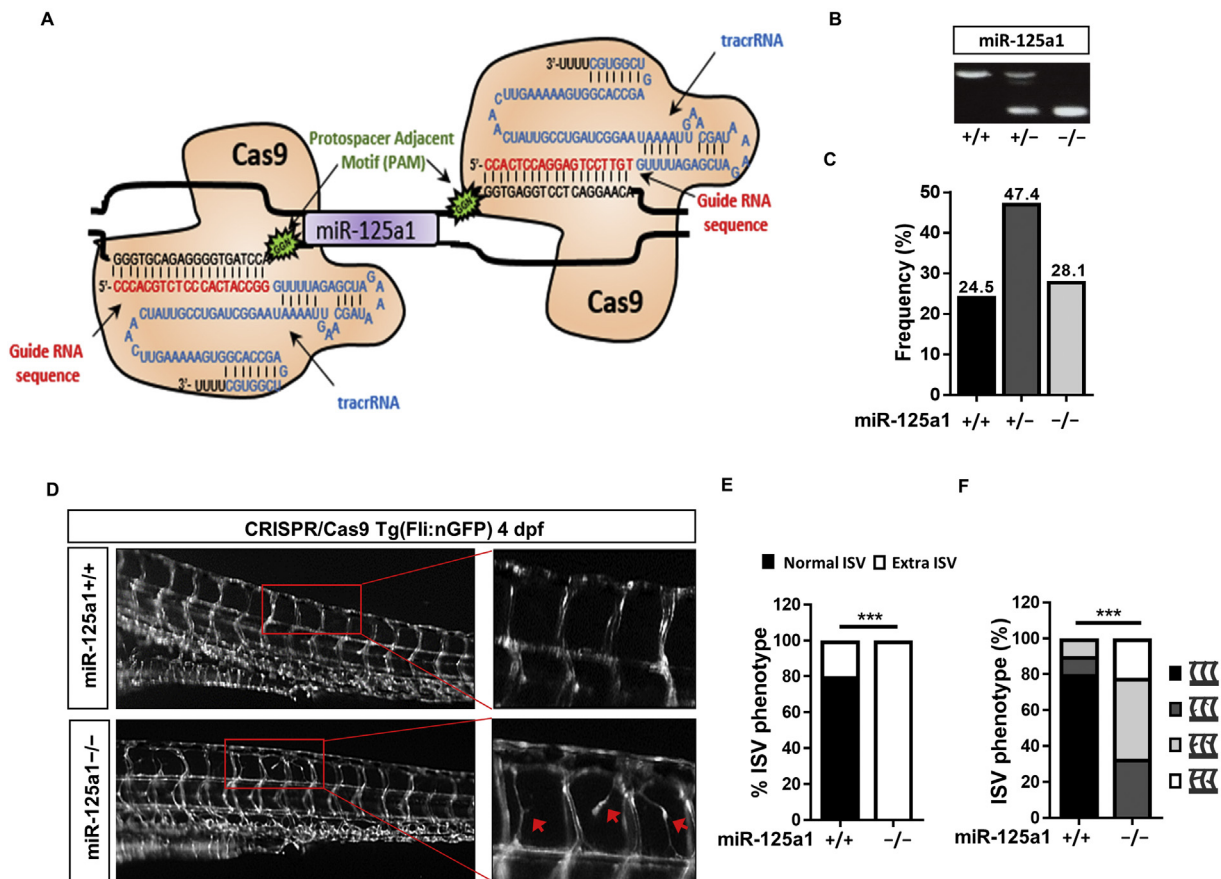

Fig. 3. miR-125a1$^{-/-}$ promote vessel sprouting. (A) Schematic representation of the generation of the miR-125a1$^{-/-}$ CRISPR/Cas9 mutants. The 5′ and 3′ regions of the zebrafish miR-125a1 gene contain protospacer adjacent motifs (PAM; Green). Guide strand RNA (red) were generated against target oligonucleotides (black) down-stream of these PAM sites. TracrRNA (blue) enables the homing of the Cas9 protein to the targeted PAM site. (B) Genotyping of miR-125a1$^{+/+}$, miR-125a1$^{+/-}$ and miR-125a1$^{-/-}$ embryos, respectively (Table S2 primer sequences). (C) The frequency of genotype variants; miR-125a1$^{+/+}$, miR-125a1$^{+/-}$ and miR-125a1$^{-/-}$ embryos, shown as a percentage of total number of incrossed miR-125a1$^{+/-}$ progeny ($n = 57$). (D) Representative image of miR-125a1$^{+/+}$ and miR125a1$^{-/-}$ embryos, showing aberrant ISV sprouting (red arrowheads) in miR-125a1$^{-/-}$ embryos. (E) The frequency of intersegmental vessel hyper-branching. (F) The incidence of no, mild, moderate and severe vascular hyper-branching caused by loss of miR-125a1. Data are represented as phenotype frequencies. *** $p < .005$ significantly different to control. See also Fig. S5.
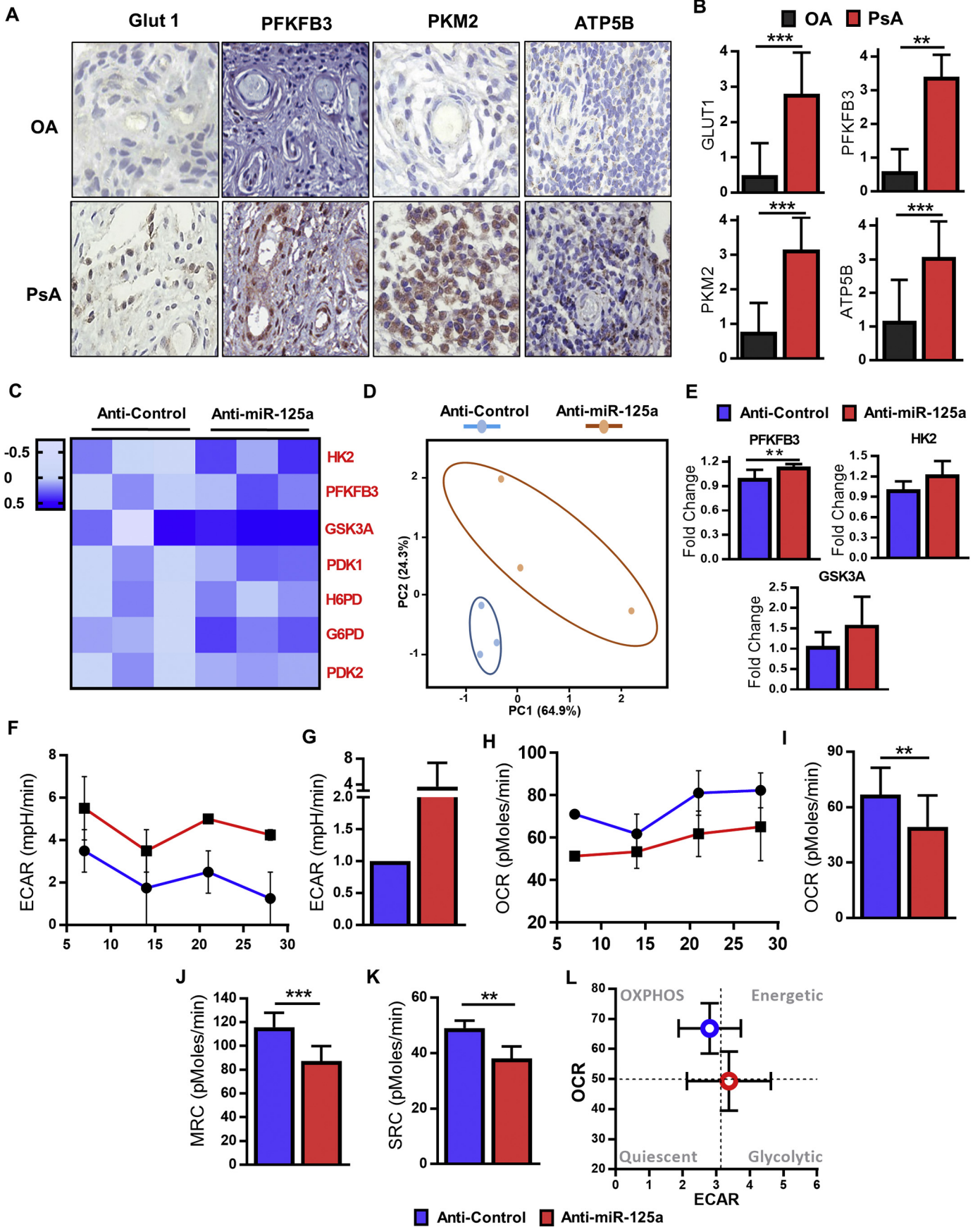
vasculature as compared to OA disease controls supporting elevated metabolism in PsA vasculature (Fig. 4A and B). Subsequent immunofluorescence staining of PsA synovial tissue demonstrated co-localisation of Von Willebrand factor (vWF) labelled vascular regions and PFKFB3 (Fig. S6).

To assess if the loss of miR-125a induces metabolic reprogramming of ECs *in vitro*, we next measured the expression of genes required for glucose metabolism (HK2, PFKFB3, GSK3A, PDK1, H6PD, G6PD and PDK2). Heatmap and principle component analysis (PCA) revealed that the loss of miR-125a results in a distinct metabolic profile from that of anti-control ECs, with an overexpression of glycolysis related genes in anti-miR-125a treated ECs (Fig. 4C and D). Notably, EC cells with reduced expression of miR-125a display increased expression of two key regulators of glycolysis, PFKFB3 and HK2, and glycogen synthesis, GSK3A (Fig. 4E), pathways crucial for EC function, particularly tumour angiogenesis [30–32]. As shown in Fig. S7, the protein expression of HK2 and PFKFB3 was also notably increased after inhibition of miR-125a in HUVEC. Higher glycolytic activity was confirmed by seahorse profiling, where the extracellular acidification rate (ECAR, a measure of glycolysis) and oxygen consumption rate (OCR, a measure of OXPHOS) were analysed 24 h post anti-miR-125a transfection, timed such that the metabolic profile was assessed while anti-miR-125a-induced angiogenesis was on-going. Anti-miR-125a ECs were distinguished from anti-control cells by a higher ECAR (Fig. 4F and G) and significantly lower baseline OCR compared to anti-control treated ECs (Fig. 4H and I). Following the serial addition of oligomycin, FCCP and antimycin A (Summarized graph Fig. S8), anti-miR-125a treated ECs showed significantly lower maximum respiratory capacity (MRC, Fig. 4J) and spare respiratory capacity (SRC, Fig. 4K) compared to anti-control treated cells. Together, these data demonstrate a distinct metabolic shift towards glycolysis in anti-miR-125a treated ECs (Fig. 4L).

3.5. Glycolysis is required for miR-125a-induced angiogenesis

Our results indicate that a glycolytic shift is necessary for miR-125a-induced angiogenic mechanisms. Therefore, we examined the impact of a PFKFB3-targeting glycolytic inhibitor, 3PO [13,14,33], on EC miR-125a-induced angiogenesis. To verify that loss of glycolytic flux prevents miR-125a-induced angiogenesis *in vivo*, we treated 3 dpf miR-125a1$^{-/-}$ embryos, timed such to capture the development of the hyper-branching phenotype, with 3PO or DMSO vehicle control. As demonstrated in Fig. 5A, the presence of 3PO attenuated vessel hyper-branching in miR-125a1$^{-/-}$ larvae 4 at dpf. While 80% of DMSO control treated miR-125a1$^{-/-}$ embryos displayed severe or moderate ISV hyper-branching, 0% of 3PO treated miR-125a1$^{-/-}$ embryos showed these phenotypes, where 20% displayed a mild phenotype and 80% displayed a completely normal ISV (Fig. 5A and B). Under anti-control conditions *in vitro*, ECs exhibited normal migration, invasion and tube formation in the presence or absence of 3PO (Fig. 5C–E). By contrast, anti-miR-125a ECs cultured in the presence of 3PO exhibited almost a complete lack of miR-125a-induced migration, invasion and tube formation (Fig. 5C–E), further verifying the requirement of glycolysis in miR-125a-mediated EC activation. Together, these data

demonstrate that EC activation in response to miR-125a deficiency is dependent upon elevated glycolysis.

4. Discussion

The majority of studies examining angiogenesis in inflammatory arthritis have focused on angiogenic factors and cytokines, however the effect of anti-angiogenic therapies such as anti-VEGF agents, have not fulfilled their expectations, with modest survival improvements in patients with cancer [34] and evidence of enhanced malignancy following vessel pruning due to elevated tumour hypoxia [35]. A more recent anti-angiogenic approach is vessel normalisation to improve vessel structure and tissue perfusion. By examining miRNA and synovial angiogenesis, we demonstrate that the bioenergetic profile of endothelial cells is integral to the functional and structural form of synovial vasculature. Decreased expression of miR-125a in PsA synovial tissue was associated with joint vascularity and induced EC activation *in vitro*. Using anti-sense morpholinos and CRISPR/Cas9 techniques, we demonstrate loss of miR-125a in zebrafish embryos mimics the hyper-vascular phenotype observed in the PsA synovium. Our results show that inhibition of endogenous miR-125a *in vitro* is sufficient to induce a distinct transcriptional metabolic signature in ECs, with increased expression of metabolic markers observed in the synovial vascular regions *ex vivo*. In particular, we found that enhanced EC glycolysis mediates miR-125a-induced angiogenic mechanisms and that inhibition of glycolysis through PFKFB3 blockade normalised the miR-125a-induced hyperbranching *in vitro* and *in vivo*. Together our data implicate miR-125a as an important regulator of joint angiogenesis and highlights metabolic reprogramming as a new opportunity to normalise synovial vasculature in inflammatory arthritis.

We demonstrated that decreased expression of miR-125a in PsA synovial tissue is associated with increased macroscopic vascularity. Consistent with this observation, studies have demonstrated decreased expression of miR-125a in EC derived from multiple sclerosis (MS) lesions, which was associated with poor barrier function and immune cell infiltration [36]. Previous work has demonstrated distinct vascular morphology in the PsA synovium characterized by a tortuous, elongated vessel, displaying an irregular hyper-branched appearance [5,37]. Functionally, they are immature and poorly perfused, resulting in PO$_2$ levels as low as 0.46% and increased trafficking of immune cells into the synovial space [38–40]. A similar vascular phenotype was observed in this study, wherein a deficiency of miR-125a *in vitro* and *in vivo* led to increased vascular hyper-branching. Interestingly, hypoxic conditions have been previously shown to induce miR-125a down-regulation in hepatocellular carcinoma cells [41], suggesting that synovial hypoxia may contribute to the dysfunctional synovial expression of miR-125a. Molecularly, at the post-transcriptional level, miR-125a has been demonstrated to directly bind to and regulate VEGFA expression [26]. Consistent with this, decreased expression of miR-125 has been associated with tumour angiogenesis and correlated with VEGFA expression levels in hepatocellular carcinoma [42], ovarian cancer [43] and gastric cancer [26]. The common vascular phenotype in both morpholino and CRISPR/Cas9 reverse genetic approaches in this study demonstrate that the miR-125a1$^{-/-}$ transgenic lines faithfully represent the pro-angiogenic

Fig. 4. miR-125a drives endothelial cell glycolysis. (A) Representative images of synovial tissue vascular expression of GLUT1, PFKFB3, PKM2 and ATP5B from patients with PsA and OA. Original magnification: 10×. (B) Semi-quantification for GLUT1, PFKFB3, PKM2 and ATP5B in the vascular region of PsA and OA patients. (C) HUVEC cells were treated with anti-miR-125a and RNA expression of genes was measured by quantitative RT-PCR. Heat map displays expression of genes with data presented as the log$_2$ value ($n = 3$). (D) Principle Component Analysis (PCA) of gene transcripts data, revealing unique clustering of anti-miR-125a treated cells compared to anti-control cells. (E) qPCR analysis of PFKB3, HK2 and GSK3A in anti-control and anti-miR-125a treated HUVEC ($n = 3$). (F) ECAR baseline rates were measured using a Seahorse Bioanalyzer following 24 h treatment with anti-miR-125a or scrambled control. Summarized graph from 3 anti-control and 3 anti-miR-125a treated HUVECs is shown. (G) Rate of ECAR in HUVECs cultured with anti-control and anti-miR-125a nucleotides. ECAR rate is expressed as a fold change relative to the ECAR measurement of anti-control transfection. (H) Summarized graph showing baseline OCR rates from anti-control and anti-miR-125a treated HUVEC ($n = 3$). Rate of baseline OCR in HUVECs treated with anti-control and anti-miR-125a ($n = 3$). Mitochondrial function was probed by the sequential addition of oligomycin, FCCP and antimycin A. (J) Maximum respiratory capacity rate in HUVECs treated with anti-control and anti-miR-125a ($n = 3$). (K) Spare respiratory capacity rate in HUVECs treated with anti-control and anti-miR-125a ($n = 3$). (L) Energy map of anti-control and anti-miR-125a treated HUVECs showing a distinct shift in anti-miR-125a HUVECs towards a glycolytic/energetic phase. ECAR: extracellular acidification rate, OCR: oxygen consumption rate, MRC: maximum respiratory capacity, SRC: spare respiratory capacity. Data are represented as mean ± SEM. *** p < .005, ** p < .01 significantly different to control. See also Fig. S6.
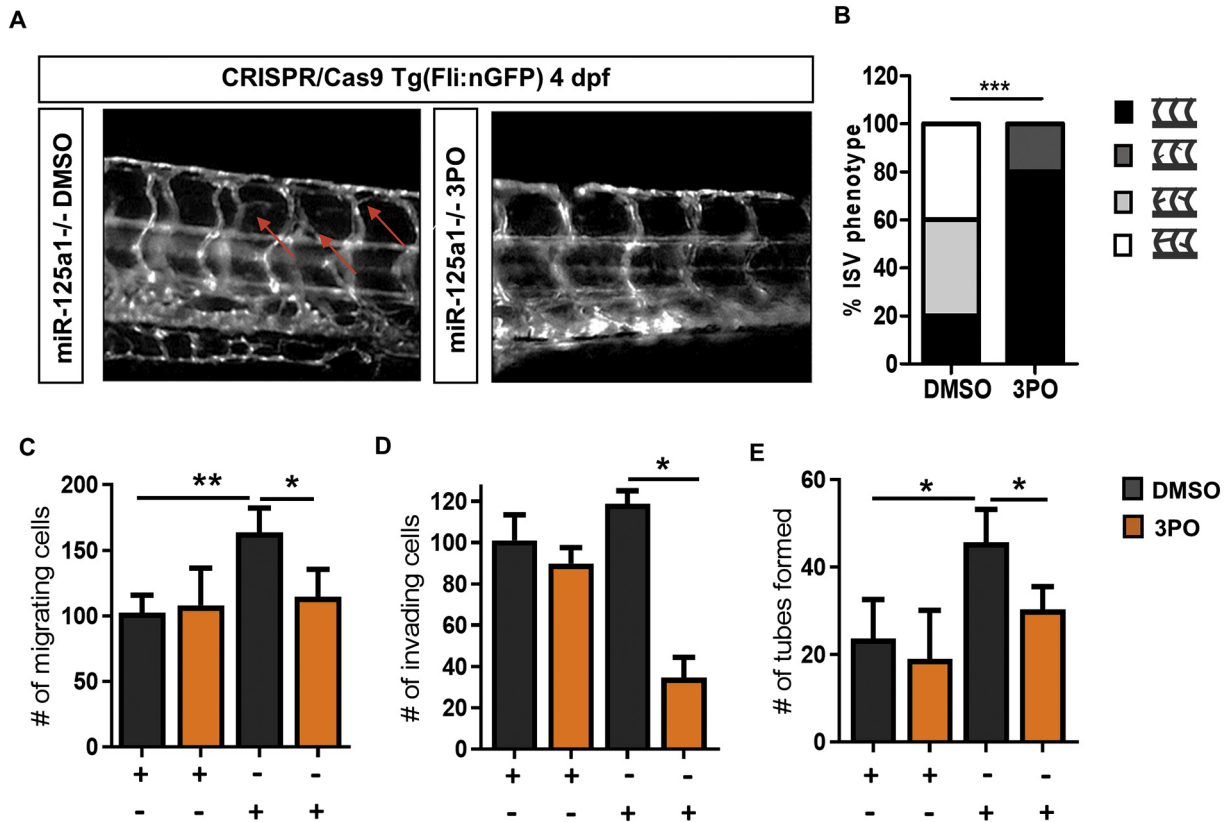
Fig. 5. Inhibition of glycolysis impairs miR-125a-induced pro-angiogenic phenotype. Bar graph quantifying the inhibition of anti-miR-125a induced cell migration (A), invasion (B) and network formation (C) in response to 3PO (n = 3). Data are represented as mean ± SEM, *p < .05, significantly different to control. (D) Representative fluorescent images demonstrating vascular hyper-branching (red arrows) in miR-125a1$^{-/-}$ embryos in the presence of DMSO (n = 5). Treatment of miR-125a1$^{-/-}$ embryos with 3PO largely normalised the hyper-branching phenotype (n = 5). (E) Incidence of phenotype severity showing the no, mild, moderate and severe hyper-vascular branching in miR-125a1$^{-/-}$ in the presence of 3PO or DMSO vehicle control. Data are presented as phenotype frequencies. Statistical significance was analysed by the chi-square test. ***p < .001, significantly different to control. See also Fig. S7.

phenotype of miR-125 knockdown activity *in vivo*. A future challenge is the direct analysis of the cell autonomous function of miR-125a−/− zebrafish in regulating angiogenesis. The importance of angiogenesis in early disease and the observed decreased expression of miR-125a associated with *in vivo* synovial vascularity in patients with PsA, suggests miR-125a may play an important role in the early stages of synovial inflammation, from initiation and development to progression towards chronic autoimmunity. While we have shown *in vitro* and *in vivo* that miR-125a deficiency regulates dysfunctional angiogenesis, and demonstrated an association of low synovial miR-125a with PsA synovial vasculature, a limitation of the study is cellular localisation of miR-125a in PsA synovial tissue, due to difficulty in isolating primary endothelial cells from synovial tissue and the challenge of detecting a lowly expressed miR-125a. Future studies examining the spatiotemporal expression of miR-125a and miR-125b in the PsA synovium, or advances in single cell analysis of PsA synovium will extend the current findings and further elucidate the co-regulatory role of miR-125a across the different cellular subsets within the synovium. While the regulatory mechanism regulating the reduced synovial expression remains to be elucidated, DNA methylation, single-nucleotide polymorphisms and translocation abnormalities within the miR-125a gene have been linked to disease development in cancer [44–46].

Previous work has established the role of metabolism in promoting mechanisms of synovial inflammation and immune cell activity [27,47–49]. Our data now also indicates increased metabolism within the vascular regions of the inflamed synovium, with elevated vascular expression of GLUT1, PFKFB3, PKM2 and ATP5B in PsA synovium compared to OA disease comparators. Gene expression studies identified a distinct glycolysis-related gene signature in miR-125a deficient ECs resulting in a metabolic shift towards glycolysis. This metabolic switch

is equivalent to mechanisms of vascular dysfunction in tumour pathogenesis [50], where it is required for EC activation and function [14]. In addition, glucose-derived carbons, *via* the pentose-phosphate pathway (PPP), enable nucleotide synthesis required for cell proliferation. In agreement, miR-125a deficient ECs exhibited increased expression of G6PD, a rate-limiting enzyme of the PPP, suggesting miR-125a-activated ECs can divert glucose-derived carbons into these pathways to sustain rapid proliferation and it's hyperbranching phenotype. Of note, miR-125a-activated ECs maintained OXPHOS, SRC and MRC, suggesting that they can still engage in mitochondrial respiration and are metabolically flexible to enable response to environmental stress and maintain cell viability.

In agreement with previous studies [26,41], we showed that a deficiency of miR-125a exhibits both a pro-angiogenic and a pro-glycolytic phenotype. Given the target multiplicity associated with miRNA biological function, it may be suggested that miR-125a simultaneously regulates both the pro-angiogenic and metabolic signalling pathways associated with dysfunctional angiogenesis in disease [8,50]. The inhibition of PFKFB3 and subsequent partial blockade of glycolysis is known to impair vessel hyper-branching and promote vessel normalisation in response to pro-angiogenic factors, such as VEGF [13,50]. In further support of this hypothesis, PFKFB3 inhibition has effectively impaired inflammation-driven angiogenesis and tumour angiogenesis in murine models, with reduced frequencies of infiltrating immune cells and reduced disease severity being observed [13,50]. We have observed that PFKFB3 inhibition induces an almost complete normalisation of the miR-125a−/− vascular phenotype and miR-125a deficient EC. This suggests that miR-125a levels in ECs may regulate their metabolic/pro-angiogenic profile to control vascular morphology and function, in particular tortuous vessels which are a key feature of the PsA vascular
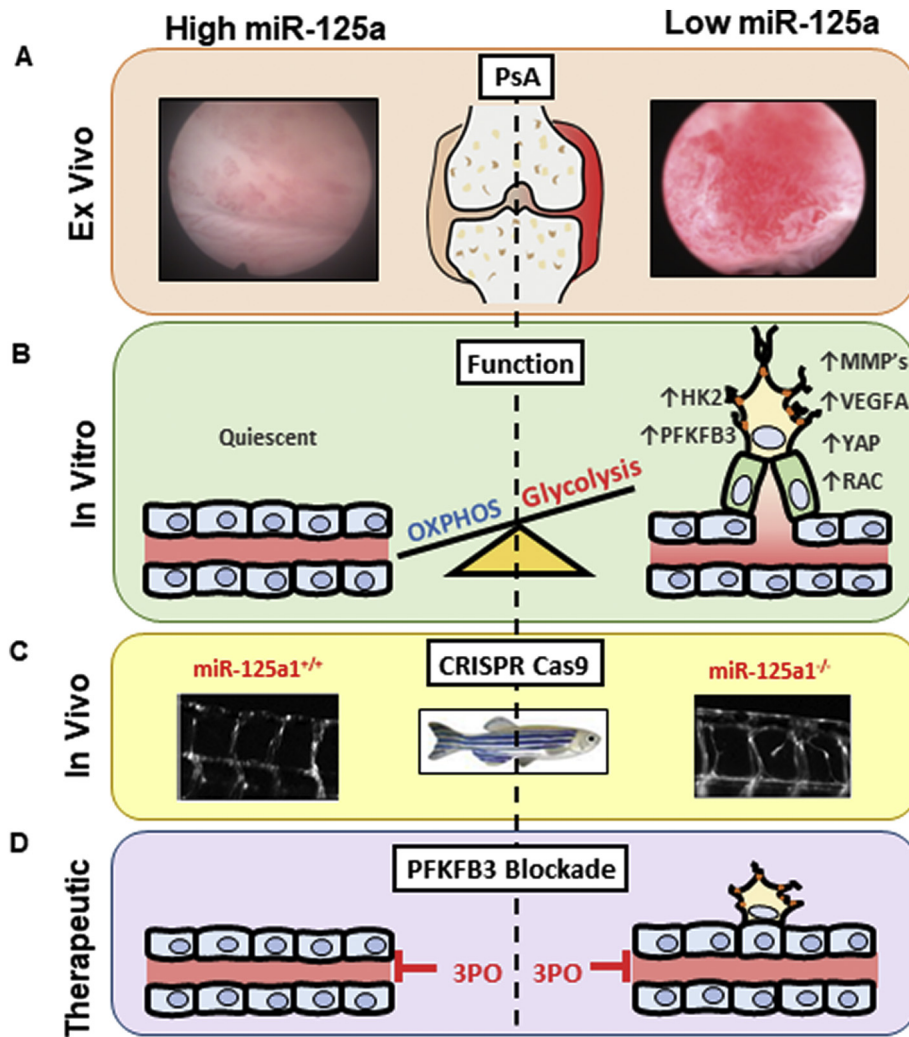
Fig. 6. Schematic diagram summarising the role of miR-125a in regulating angiogenesis. (A) Low miR-125a is associated with increased macroscopic synovial vasculature in PsA patients in vivo. (B) MiR-125a deficiency promotes endothelial cell activation and sprout formation *in vitro*. (C) MiR-125a deficiency promotes vascular hyperbranching in a zebrafish model. (D) Blockade of glycolytic enzyme PFKFB3 with 3PO induces vessel normalisation.

phenotype. However, it is important to note that DMSO treated miR-125a−/− larvae showed an increase in the frequency of severe hyperbranching, with a parallel decrease in the frequency of mild hyperbranching, suggesting that a more aggressive hyperbranching phenotype in the presence of DMSO. These relative differences in phenotype frequencies, could be partially a reflection of the global effects of DMSO as a solvent. Together, these data support the miR-125a-glycoylsis axis (Fig. 6) as a new opportunity for anti-angiogenic intervention in PsA and other angiogenesis driven diseases.

Author contribution

SW- Literature search, figures, study design, data collection, data analysis, data interpretation, writing of manuscript, and, edits to final submitted manuscript.

NO-Literature search, study design, data collection, data analysis, data interpretation, edits to final submitted manuscript.

HMcL- Data collection, data analysis, data interpretation, edits to final submitted manuscript.

MB- Data collection, data analysis, data interpretation, edits to final submitted manuscript.

SPC- Data collection, data analysis, data interpretation, edits to final submitted manuscript.

MT-Study design, data analysis, data interpretation, edits to final submitted manuscript.

CCC- Data collection, data analysis, data interpretation, edits to final submitted manuscript.

TMcG- Data collection, data analysis, data interpretation, edits to final submitted manuscript.

MC- Data collection, data analysis, data interpretation, edits to final submitted manuscript.

BNK-Study design, data analysis, data interpretation, edits to final submitted manuscript.

DJV- Study design, figures, data collection, data analysis, data interpretation, edits to final submitted manuscript.

UF- Literature search, Figures, study design, data analysis, data interpretation, writing of manuscript, final approval of submitted manuscript.

Declaration of Competing Interest

No conflicts of interest.

Acknowledgements

Appendix A. Supplementary data

Supplementary data to this article can be found online at https://doi.org/10.1016/j.ebiom.2019.08.043.

References

[1] Veale DJ, Ritchlin C, FitzGerald O. Immunopathology of psoriasis and psoriatic arthritis. Ann Rheum Dis 2005;64(Suppl. 2):ii26–9.

[2] Saber TP, Ng CT, Renard G, Lynch BM, Pontifex E, Walsh CAE, et al. Remission in psoriatic arthritis: is it possible and how can it be predicted? Arthritis Res Ther 2010;12:R94.

[3] Rooney M, Condell D, Quinlan W, Daly L, Whelan A, Feighery C, et al. Analysis of the histologic variation of synovitis in rheumatoid arthritis. Arthritis Rheum 1988;31:956–63.

[4] Kennedy A, Ng CT, Chang TC, Biniecka M, O'Sullivan JN, Heffernan E, et al. Tumor necrosis factor blocking therapy alters joint inflammation and hypoxia. Arthritis Rheum 2011;63:923–32.

[5] Reece RJ, Canete JD, Parsons WJ, Emery P, Veale DJ. Distinct vascular patterns of early synovitis in psoriatic, reactive, and rheumatoid arthritis. Arthritis Rheum 1999;42:1481–4.

[6] Moll C, Bogas M, Gómez-Puerta JA, Celis R, Vázquez I, Rodríguez F, et al. Macroscopic features of knee synovitis in early untreated Behçet disease and psoriatic arthritis. Clin Rheumatol 2009;28:1053–7.

[7] Fearon U, Reece R, Smith J, Emery P, Veale DJ. Synovial cytokine and growth factor regulation of MMPs/TIMPs: implications for erosions and angiogenesis in early rheumatoid and psoriatic arthritis patients. Ann N Y Acad Sci 1999;878:619–21.

[8] Fearon U, Griosios K, Fraser A, Reece R, Emery P, Jones PF, et al. Angiopoietins, growth factors, and vascular morphology in early arthritis. J Rheumatol 2003;30:260–8.

[9] Clavel G, Bessis N, Lemeiter D, Fardellone P, Mejjad O, Ménard J-F, et al. Angiogenesis markers (VEGF, soluble receptor of VEGF and angiopoietin-1) in very early arthritis and their association with inflammation and joint destruction. Clin Immunol 2007;124:158–64.

[10] Ballara S, Taylor PC, Reusch P, Marm D, Feldmann M, Maini RN, et al. Raised serum vascular endothelial growth factor levels are associated with destructive change in inflammatory arthritis. Arthritis Rheum 2001;44:2055–64 John Wiley & Sons, Inc.

[11] Chong V. Ranibizumab for the treatment of wet AMD: a summary of real-world studies. Eye Nature Publishing Group 2016;30:270–86.

[12] Welti J, Loges S, Dimmeler S, Carmeliet P. Recent molecular discoveries in angiogenesis and antiangiogenic therapies in cancer. J Clin Invest 2013;123:3190–200.

[13] Schoors S, De Bock K, Cantelmo AR, Georgiadou M, Ghesquière B, Cauwenberghs S, et al. Partial and transient reduction of glycolysis by PFKFB3 blockade reduces pathological angiogenesis. Cell Metab 2014;19:37–48.

[14] De Bock K, Wong BW, Cantelmo AR, Quaegebeur A, Ghesquiè Re B, Cauwenberghs S, et al. Role of PFKFB3-driven glycolysis in vessel sprouting. Cell Stefan Vinckier 2013;154:651–63.

[15] Goveia J, Stapor P, Carmeliet P. Principles of targeting endothelial cell metabolism to treat angiogenesis and endothelial cell dysfunction in disease. EMBO Mol Med 2014;6:1105–20.

[16] McGarry T, Biniecka M, Gao W, Cluxton D, Canavan M, Wade S, et al. Resolution of TLR2-induced inflammation through manipulation of metabolic pathways in Rheumatoid Arthritis. Sci Rep 2017;7:43165.

[17] Conradi L-C, Brajic A, Cantelmo AR, Bouché A, Kalucka J, Pircher A, et al. Tumor vessel disintegration by maximum tolerable PFKFB3 blockade. Angiogenesis 2017;20:599–613.

[18] Watanabe R, Shirai T, Namkoong H, Zhang H, Berry GJ, Wallis BB, et al. Pyruvate controls the checkpoint inhibitor PD-L1 and suppresses T cell immunity. J Clin Invest 2017;127:2725–38.

[19] Wade SM, Trenkmann M, McGarry T, Canavan M, Marzaioli V, Wade SC, et al. Altered expression of microRNA-23a in psoriatic arthritis modulates synovial fibroblast proinflammatory mechanisms via phosphodiesterase 4B. J Autoimmun 2019;96:86–93.

[20] Podshivalova K, Salomon DR. MicroRNA regulation of T-lymphocyte immunity: modulation of molecular networks responsible for T-cell activation, differentiation, and development. Crit Rev Immunol 2013;33:435–76.

[21] Rottiers V, Näär AM. MicroRNAs in metabolism and metabolic disorders. Nat Rev Mol Cell Biol 2012;13:239–50 Nature Publishing Group.

[22] Le Bot N. MicroRNAs in angiogenesis. Nat Cell Biol Nat Res Forum 2012;14:342.

[23] Ciancio G, Ferracin M, Saccenti E, Bagnari V, Farina I, Furini F, et al. Characterisation of peripheral blood mononuclear cell microRNA in early onset psoriatic arthritis. Clin Exp Rheumatol 2017;35:113–21.

[24] Chatzikyriakidou A, Voulgari PV, Georgiou I, Drosos AA. The role of microRNA-146a (miR-146a) and its target IL-1R-associated kinase (IRAK1) in psoriatic arthritis susceptibility. Scand J Immunol 2010;71:382–5.

[25] Muramatsu F, Kidoya H, Naito H, Sakimoto S, Takakura N. microRNA-125b inhibits tube formation of blood vessels through translational suppression of VE-cadherin. Oncogene Nature 2013;32:414–21 Publishing Group.

[26] Dai J, Wang J, Yang L, Xiao Y, Ruan Q. miR-125a regulates angiogenesis of gastric cancer by targeting vascular endothelial growth factor A. Int J Oncol 2015;47:1801–10.

[27] Biniecka M, Canavan M, McGarry T, Gao W, McCormick J, Cregan S, et al. Dysregulated bioenergetics: a key regulator of joint inflammation. Ann Rheum Dis BMJ Publish Group Ltd 2016;75:2192–200.

[28] Cantelmo AR, Brajic A, Carmeliet P. Endothelial metabolism driving angiogenesis. Cancer J 2015;21:244–9.

[29] Eelen G, de Zeeuw P, Simons M, Carmeliet P. Endothelial cell metabolism in normal and diseased vasculature. Circ Res 2015;116.

[30] Cantelmo AR, Conradi L-C, Brajic A, Goveia J, Kalucka J, Pircher A, et al. Inhibition of the glycolytic activator PFKFB3 in endothelium induces tumor vessel normalization, impairs metastasis, and improves chemotherapy. Cancer Cell 2016;30:968–85.

[31] Zhao P, Li Q, Shi Z, Li C, Wang L, Liu X, et al. GSK-3B regulates tumor growth and angiogenesis in human glioma cells. Oncotarget 2015;6:31901–15.

[32] Eelen G, Dubois C, Cantelmo AR, Goveia J, Brüning U, DeRan M, et al. Role of glutamine synthetase in angiogenesis beyond glutamine synthesis. Nature 2018;561:63–9.

[33] Clem B, Telang S, Clem A, Yalcin A, Meier J, Simmons A, et al. Small-molecule inhibition of 6-phosphofructo-2-kinase activity suppresses glycolytic flux and tumor growth. Mol Cancer Ther 2008;7:110–20.

[34] Jayson GC, Kerbel R, Ellis LM, Harris AL. Antiangiogenic therapy in oncology: current status and future directions. Lancet Elsevier 2016;388:518–29.

[35] Loges S, Schmidt T, Carmeliet P. Mechanisms of resistance to anti-angiogenic therapy and development of third-generation anti-angiogenic drug candidates. Genes Cancer Impact J 2010;1:12–25.

[36] Reijerkerk A, Lopez-Ramirez MA, van het Hof B, Drexhage JAR, Kamphuis WW, Kooij G, et al. MicroRNAs regulate human brain endothelial cell-barrier function in inflammation: implications for multiple sclerosis. J Neurosci 2013;33:6857–63.

[37] Veale D, Yanni G, Rogers S, Barnes L, Bresnihan B, Fitzgerald O. Reduced synovial membrane macrophage numbers, ELAM-1 expression, and lining layer hyperplasia in psoriatic arthritis as compared with rheumatoid arthritis. Arthritis Rheum 1993;36:893–900.

[38] Kennedy A, Ng CT, Biniecka M, Saber T, Taylor C, O'Sullivan J, et al. Angiogenesis and blood vessel stability in inflammatory arthritis. Arthritis Rheum 2010;62:711–21.

[39] Ng CT, Biniecka M, Kennedy A, McCormick J, FitzGerald O, Bresnihan B, et al. Synovial tissue hypoxia and inflammation in vivo. Ann Rheum Dis 2010;69:1389–95.

[40] Biniecka M, Connolly M, Gao W, Ng CT, Balogh E, Gogarty M, et al. Redox-mediated angiogenesis in the hypoxic joint of inflammatory arthritis. Arthritis Rheum 2014;66:3300–10.

[41] Jin F, Wang Y, Zhu Y, Li S, Liu Y, Chen C, et al. The miR-125a/HK2 axis regulates cancer cell energy metabolism reprogramming in hepatocellular carcinoma. Sci Rep 2017;7:3089.

[42] Bi Q, Tang S, Xia L, Du R, Fan R, Gao L, et al. Ectopic expression of MiR-125a inhibits the proliferation and metastasis of hepatocellular carcinoma by targeting MMP11 and VEGF. Wong C-M PLoS One 2012;7:e40169 Public Library of Science.

[43] He J, Jing Y, Li W, Qian X, Xu Q, Li F-S, et al. Roles and mechanism of miR-199a and miR-125b in tumor angiogenesis. Cheng JQ, editor PLoS One 2013;8:e56647.

[44] Duan R, Pak C, Jin P. Single nucleotide polymorphism associated with mature miR-125a alters the processing of pri-miRNA. Hum Mol Genet 2007;16:1124–31.

[45] Bousquet M, Quelen C, Rosati R, Mansat-De Mas V, La Starza R, Bastard C, et al. Myeloid cell differentiation arrest by miR-125b-1 in myelodysplastic syndrome and acute myeloid leukemia with the t(2;11)(p21;q23) translocation. J Exp Med 2008;205:2499–506 The Rockefeller University Press.

[46] Chen H, Xu Z. Hypermethylation-associated silencing of miR-125a and miR-125b: a potential marker in colorectal cancer. Dis Markers Hindawi Limited 2015;2015:345080.

[47] Shi LZ, Wang R, Huang G, Vogel P, Neale G, Green DR, et al. HIF1alpha-dependent glycolytic pathway orchestrates a metabolic checkpoint for the differentiation of TH17 and Treg cells. J Exp Med 2011;208:1367–76 The Rockefeller University Press.

[48] Krawczyk CM, Holowka T, Sun J, Blagih J, Amiel E, DeBerardinis RJ, et al. Toll-like receptor-induced changes in glycolytic metabolism regulate dendritic cell activation. Blood Am Soc Hematol 2010;115:4742–9.

[49] Zeisbrich M, Yanes RE, Zhang H, Watanabe R, Li Y, Brosig L, et al. Hypermetabolic macrophages in rheumatoid arthritis and coronary artery disease due to glycogen synthase kinase 3b inactivation. Ann Rheum Dis 2018;77:1053–62 BMJ Publishing Group Ltd.

[50] Missiaen R, Morales-Rodriguez F, Eelen G, Carmeliet P. Targeting endothelial metabolism for anti-angiogenesis therapy: A pharmacological perspective. Vascul Pharmacol Mar 2017;90:8–18.

[51] Taylor W, Gladman D, Helliwell P, Marchesoni A, Mease P, Mielants H. Classification criteria for psoriatic arthritis: development of new criteria from a large international study. Arthritis Rheum 2006;54:2665–73.

[52] Chen C, D a Ridzon, Broomer AJ, Zhou Z, Lee DH, Nguyen JT, et al. Real-time quantification of microRNAs by stem-loop RT-PCR. Nucleic Acids Res 2005;33:e179.

[53] Connolly M, Veale DJ, Fearon U. Acute serum amyloid a regulates cytoskeletal rearrangement, cell matrix interactions and promotes cell migration in rheumatoid arthritis. Ann Rheum Dis 2011;70:1296–303.

[54] Youssef PP, Kraan M, Breedveld F, Bresnihan B, Cassidy N, Cunnane G, et al. Quantitative microscopic analysis of inflammation in rheumatoid arthritis synovial membrane samples selected at arthroscopy compared with samples obtained blindly by needle biopsy. Arthritis Rheum 1998;41:663–9 John Wiley & Sons, Inc.

[55] Mullan RH, McCormick J, Connolly M, Bresnihan B, Veale DJ, Fearon U.. A role for the high-density lipoprotein receptor SR-B1 in synovial inflammation via serum amyloid-A. Am J Pathol Apr 2010;176(4):1999–2008.

[56] Sander JD, Maeder ML, Reyon D, Voytas DF, Joung JK, Dobbs D. ZiFiT (Zinc Finger Targeter): an updated zinc finger engineering tool. Nucleic Acids Res 2010;38: W462–8 Oxford University Press.

[57] Sander JD, Zaback P, Joung JK, Voytas DF, Dobbs D. Zinc Finger Targeter (ZiFiT): an engineered zinc finger/target site design tool. Nucleic Acids Res 2007;35: W599–605 Oxford University Press.

[58] Hwang WY, Fu Y, Reyon D, Maeder ML, Tsai SQ, Sander JD, et al. Efficient genome editing in zebrafish using a CRISPR-Cas system. Nat Biotechnol 2013;31:227–9.